Atmos. Meas. Tech. Discuss., 6, 10021–10056, 2013
www.atmos-meas-tech-discuss.net/6/10021/2013/
doi:10.5194/amtd-6-10021-2013

Atmospheric Measurement Techniques Discussions

Assessment of cloud supersaturation by aerosol particle and cloud condensation nuclei (CCN) measurements

M. L. Krüger[1], S. Mertes[2], T. Klimach[1], Y. Cheng[1], H. Su[1], J. Schneider[1], M. O. Andreae[1], U. Pöschl[1], and D. Rose[1]

[1]Max Planck Institute for Chemistry, P.O. Box 3060, 55020 Mainz, Germany
[2]Leibniz Institute for Tropospheric Research, Permoserstraße 15, 04318 Leipzig, Germany

Received: 19 September 2013 – Accepted: 8 November 2013 – Published: 15 November 2013

Correspondence to: D. Rose (d.rose@mpic.de)

Published by Copernicus Publications on behalf of the European Geosciences Union.

Abstract

In this study we show how size-resolved measurements of aerosol particles and cloud condensation nuclei (CCN) can be used to characterize the supersaturation of water vapor in a cloud. The method was developed and applied for the investigation of a cloud event during the ACRIDICON-Zugspitze campaign (17 September to 4 October 2012) at the high-alpine research station Schneefernerhaus (German Alps, 2650 m a.s.l.). Number size distributions of total and interstitial aerosol particles were measured with a scanning mobility particle sizer (SMPS), and size-resolved CCN efficiency spectra were recorded with a CCN counter system operated at different supersaturation levels.

During the evolution of a cloud, aerosol particles are exposed to different supersaturation levels. We outline and compare different estimates for the lower and upper bounds (S_{low}, S_{high}) and the average value (S_{avg}) of peak supersaturation encountered by the particles in the cloud. For the investigated cloud event, we derived $S_{low} \approx 0.19$–$0.25\,\%$, $S_{high} \approx 0.90$–$1.64\,\%$ and $S_{avg} \approx 0.38$–$0.84\,\%$. Estimates of S_{low}, S_{high} and S_{avg} based on aerosol size distribution data require specific knowledge or assumptions of aerosol hygroscopicity, which are not required for the derivation of S_{low} and S_{avg} from the size-resolved CCN efficiency spectra.

1 Introduction

Atmospheric aerosols consist of particles spanning a wide range of size and chemical composition from various natural and anthropogenic sources (Pöschl, 2005). They can act as cloud condensation nuclei (CCN) and affect climate by influencing the properties of clouds and precipitation (Lohmann and Feichter, 2005; Solomon et al., 2007; Rosenfeld et al., 2008). The water vapor supersaturation at which aerosol particles are activated as CCN depends on particle size, composition and mixing state (e.g., Köhler, 1936; Dusek et al., 2006; McFiggans et al., 2006; Andreae and Rosenfeld, 2008; Su et al., 2010).

As a result of long-term efforts and recent advances in atmospheric research, the CCN activity of atmospheric aerosol particles can be fairly well constrained by measurements and models (e.g., Petters and Kreidenweis, 2007, 2008; Gunthe et al., 2009; Kinne, 2009; Moore and Nenes, 2009; Pöschl et al., 2009; Jurányi et al., 2010; Pringle et al., 2010; Rose et al., 2010, 2011; Wex et al., 2010, 2011; Gunthe et al., 2011; Kim et al., 2011; Kulmala et al., 2011; Spracklen et al., 2011; Anttila et al., 2012; Christensen and Petters, 2012; Engelhart et al., 2012; Padró et al., 2012; Jurányi et al., 2013; Lance et al., 2013; Mikhailov et al., 2013; Petters and Kreidenweis, 2013). To fully describe the process of CCN activation and cloud droplet growth in the atmosphere, however, also the supersaturation of water vapor in the cloud needs to be known (e.g., Reutter et al., 2009; Pruppacher and Klett, 2010; Rosenfeld et al., 2012; Renno et al., 2013).

Upon cloud formation, the decrease of temperature in an ascending air parcel arising from the expansion of air with decreasing pressure (adiabatic cooling) or the decrease of temperature in an air parcel moving horizontally over a colder surface or air mass (isobaric cooling) induces water vapor supersaturation (Pruppacher and Klett, 2010). At the point where the increase of supersaturation by cooling is compensated by the condensational sink of water vapor, the supersaturation reaches a maximum or peak value. Following Hammer et al. (2013) we use the expression "peak" rather than "maximum" supersaturation. Particles with a critical supersaturation equal to or lower than the peak supersaturation are activated and grow into cloud droplets. The peak supersaturation is a major determinant for the cloud droplet number and the regime of CCN activation (aerosol- vs. updraft-limited; Reutter et al., 2009; Rosenfeld et al., 2012). Due to inhomogeneities of the atmospheric aerosol load and air flow pattern (turbulence, entrainment), the peak supersaturations of different air parcels in a cloud can be temporally and spatially heterogeneous.

Techniques for the direct measurement of cloud supersaturation are not available. Thus, indirect methods have been developed to estimate the value of water vapor

supersaturation in a cloud, which determines the fraction of particles that are activated and form cloud droplets.

An early approach to deduce the cloud supersaturation was presented by Hoppel et al. (1996). They commonly observed a double-peaked structure of the aerosol size distribution in the marine boundary layer, which is a result of processing aerosol through non-precipitating cloud cycles. The authors suggest that the mode that peaks at 20 to 80 nm consists of particles that are too small to be activated during the cloud processing, and the mode that peaks at 160 to 400 nm represents the residue of evaporated cloud droplets that have been enlarged mainly as a result of liquid phase conversion of soluble trace gases to non-volatile compounds. Therefore, they could relate the diameter at which the minimum occurs (the so-called Hoppel minimum) to the supersaturation of the cloud assuming a mixture of ammonium sulfate and sulfuric acid.

Another method to derive the supersaturation of a cloud was used by e.g., Hammer et al. (2013), Ditas et al. (2012), Asmi et al. (2012), and Anttila et al. (2009). In these studies the fraction of activated particles in a cloud was deduced from the comparison of the number size distribution of interstitial particles (i.e., particles not taken up into cloud droplets) and total aerosol particles (i.e., cloud residuals plus interstitial particles). Through Köhler theory and with the assumption of an average particle hygroscopicity the diameter at which 50 % of all particles activated was related to the particles' critical supersaturation, which was then regarded as the supersaturation at which ambient clouds are formed.

In a recent study, Russell et al. (2013) measured the CCN activation of cloud residuals, which were sampled behind a counterflow virtual impactor (CVI) and compared it to the measured cloud droplet number concentration (CDNC). The supersaturation at which the CDNC was equal to the CCN concentration of the cloud residuals was assumed to be the cloud supersaturation.

Most likely the particles of a cloud are processed through a number of non-precipitating cloud cycles (typically of the order of 10 or more; Hoppel et al., 1996). Thus, different particles may have been exposed to different peak supersaturations, at

which they were activated into cloud droplets. For that reason the activation of aerosol particles in the cloud cannot be described or reproduced with the activation at one single supersaturation level.

In this study we derive and compare different estimates for an effective average value (S_{avg}) and the lower and upper bounds (S_{low}, S_{high}) of the peak supersaturation encountered by the particles in the cloud. Estimates of S_{avg} (Sects. 3.2.1 and 3.2.2), S_{low} (Sect. 3.2.3) and S_{high} (Sect. 3.2.4) based on aerosol size distribution data require specific assumptions or measurements of aerosol hygroscopicity, which are not required for the derivation of S_{low} (Sect. 3.1.1) and S_{avg} (Sect. 3.1.2) from size-resolved CCN efficiency spectra.

2 Experimental methods and data analysis

2.1 Measurement site

Measurements were performed during the ACRIDICON-Zugspitze campaign (17 September to 4 October 2012) at the research station Schneefernerhaus, a mountain site in the German Alps (47.42° N, 10.97° E, 2650 m a.s.l.; www.schneefernerhaus.de). The aim of this campaign was the investigation of liquid water clouds. For the analysis in this paper we chose one exemplary cloud event, which occurred on 19 September 2012. In the following, the time when a cloud was present at the inlet is referred to as "in-cloud" conditions and the time directly after the cloud event, when there was clearly no cloud present at the inlet, is referred to as "out-of-cloud" conditions. During in-cloud conditions the liquid water content (LWC) as measured by a particle volume monitor (Gerber, 1991) was $> 0.024\,g\,m^{-3}$ for 85 % of the time (arithmetic mean value of $0.073\,g\,m^{-3}$). This is in accordance to Henning et al. (2002) who defined a cloud event when the LWC was $> 0.02\,g\,m^{-3}$ for 85 % of the time.

2.2 Inlet system

We used an inlet segregating hydrometeors by a cyclone with a 2.5 µm cut-off ($PM_{2.5}$). During out-of-cloud conditions the inlet samples all aerosol particles with diameter < 2.5 µm (total aerosol). During in-cloud conditions particles that have been activated to cloud droplets are pre-segregated because they are larger than the inlet cut-off diameter (Mertes et al., 2005). Therefore the sampled aerosol can be regarded as interstitial.

2.3 Size-resolved CCN measurements

The number concentration of CCN was measured using a continuous-flow streamwise thermal gradient CCN counter (CCNC), commercially available from Droplet Measurement Technologies, Inc. (DMT, CCN-100). The operation principle of the CCNC is based on the fact that diffusion of heat in air is slower than diffusion of water vapor. This allows the generation of a supersaturated area inside a flow tube by combining a temperature gradient with water vapor from a continuously wetted porous inner surface (Roberts and Nenes, 2005). The inlet flow rate of the CCNC was $0.5\,L\,min^{-1}$ with a sheath-to-aerosol flow ratio of 10. The water pump was operated at a drip rate of $4\,mL\,h^{-1}$ corresponding to the CCNC setting of "low" liquid flow. By changing the temperature gradient, the supersaturation of the CCNC was set to different values between 0.06 % and 0.60 %. Particles with a critical supersaturation equal to or smaller than the prescribed supersaturation (S_{presc}) were activated and formed water droplets. An optical particle counter (OPC) at the exit of the flow tube determined the concentration of droplets larger 1 µm, which were considered to be activated CCN.

Combining the CCNC described above with a differential mobility analyzer (DMA) and a condensation particle counter (CPC), size-resolved CCN efficiency spectra at a given S_{presc} were measured as follows (Frank et al., 2006): first, aerosol particles were brought to charge equilibrium with an x-ray source (TSI 3087). Then the DMA selected monodisperse particles of 10 different diameters in the size range of 23 to

321 nm, which were passed on to the CCNC and the CPC (TSI 3762) measuring in parallel. At each diameter D, the CPC measured the number concentration of all aerosol particles (N_{CN}), and the CCNC measured the number concentration of CCN (N_{CCN}) for the given supersaturation. The CCN efficiency spectrum is the size-resolved fraction of all activated particles as a function of S_{presc}. The recording of a CCN efficiency spectrum at a given S_{presc} took ~ 23 min, including ~ 90 s integration time for each measurement data point, ~ 30 s adjustment time for each new particle size, and ~ 4 min for adjustment to the next supersaturation level. The completion of a full measurement cycle comprising CCN efficiency spectra at 5 different supersaturation levels took ~ 2 h (including additional 5 min of adjustment time between the highest and the lowest S_{presc} level).

The measurement data of the CCN efficiency spectra were corrected for differences in the CCNC and CPC counting efficiencies as described in Rose et al. (2010), using a constant correction factor of 1.03. Moreover a correction for multiple charged particles was performed according to Frank et al. (2006).

The supersaturation in the CCNC was calibrated using ammonium sulfate particles before, during and after the campaign. We used the calibration method described in Rose et al. (2008), applying the activity parameterization Köhler model AP3 to derive the corresponding critical supersaturation from the critical dry diameter of CCN activation of the ammonium sulfate particles.

To relate the activation of aerosol particles in the CCNC to the activation at ambient conditions, the supersaturation levels prescribed in the CCNC at a sample temperature of approximately 298 K (S_{presc}) were scaled to an equivalent supersaturation at an average ambient air temperature during the cloud event of ~ 273 K (S_{CCNC}) as described in Appendix C.

2.4 Error analysis

During a cloud event the number concentration measured for large monodisperse interstitial aerosol particles is generally very low. Therefore the possible sources of errors

are particularly important. One potential source for systematical errors are false counts of the instruments. However, during frequently performed zero filter tests our instruments showed no false counts, so that the systematic error initiated from false counts could be neglected. The random error of the particle concentration measured by the CCNC (ΔN_{CCN}) and by the CPC (ΔN_{CN}), as well as the random error of the activated fraction ($\Delta(N_{CCN}/N_{CN})$) were derived through Gaussian error propagation.

Hence, the error of the activated fraction is given by:

$$\Delta\left(\frac{N_{CCN}}{N_{CN}}\right) = \sqrt{\left(\frac{\Delta N_{CCN}}{N_{CN}}\right)^2 + \left(\frac{N_{CCN}\cdot\Delta N_{CN}}{N_{CN}^2}\right)^2} \quad (1)$$

in which N_{CCN} and N_{CN} are the concentrations per size bin measured during the integration interval by the CCNC and the CPC, respectively. The number concentration of particles is the number of measured particles (c) divided by the sample volume: $N = c/(Q\cdot t)$, where Q is the volumetric flow rate and t is the integration time. From this, the errors of the particle concentrations (ΔN_{CCN} and ΔN_{CN}) are given by:

$$\Delta N = \sqrt{\left(\frac{\Delta c}{Q\cdot t}\right)^2 + \left(\frac{c\cdot\Delta Q}{Q^2\cdot t}\right)^2 + \left(\frac{c\cdot\Delta t}{Q\cdot t^2}\right)^2} \quad (2)$$

Note that for the volumetric flow rate in the CCNC we had to insert the value for the measured actual aerosol flow (~ 0.045 L min^{-1}) through the flow tube. This is only 1/11 of the CCNC inlet flow since the inlet flow is split into a filtered sheath and an aerosol flow with a ratio of 10. For the measurement time t we inserted the integration time for N_{CCN} and N_{CN} at a given D and S_{CCNC} (~ 90 s). The error of the flow rate (ΔQ) was the standard deviation of the mean aerosol flow rate (of the CCNC or CPC) during time t, and the error of the time (Δt) we assumed to be 1 s.

The error of the measured particle number (c) we assumed to be the standard counting error of c plus one because one particle is the smallest countable value of the

CCNC and the CPC:

$$\Delta c = \sqrt{c + 1} \quad (3)$$

The analysis showed that the error of the interstitial CCN to CN ratio (N_{CCN}/N_{CN}) measured during a cloud event was rather large. The reason was the very small aerosol flow through the CCNC ($\sim 0.045\,L\,min^{-1}$), which required relatively long integration times.

During out-of-cloud conditions we have not encountered problems with counting statistics since the particle concentrations per size bin were at least one order of magnitude higher than during in-cloud conditions. We conclude that in future studies measuring the size-resolved CCN fraction of interstitial particles in a cloud it is necessary to increase the actual measured number of particles either by measuring over a longer time interval or by increasing the aerosol flow through the CCNC.

2.5 Calculation of CCN size distribution and integral CCN efficiency

Parallel to the CCN measurements a scanning mobility particle sizer (SMPS, TSI 3080, using a DMA 3081, a CPC 3025A, and a neutralizer 3087; operating with standard TSI software) was operated to measure the aerosol particle number (CN) size distribution over the size range of 16 to 600 nm (26 logarithmically equidistant size bins). Integral CN concentrations, $N_{CN,\,int}$, were calculated by integrating the CN size distributions.

CCN size distributions were calculated by multiplying the best-fit cumulative Gaussian distribution function (cf. Rose et al., 2008) of CCN efficiency spectra with the relevant total aerosol size distributions, which were interpolated on a grid of 250 size steps (Rose et al., 2010). Integral CCN concentrations, $N_{CCN,\,int}$, were calculated by integrating the CCN size distributions. Integral CCN efficiencies ($N_{CCN,\,int}/N_{CN,\,int}$) were calculated as the ratio of integral CCN concentration at a certain S_{CCNC} to integral CN concentration.

A list of frequently used symbols is given in Table A1 at the end of the manuscript.

3 Results and discussion

3.1 Derivation of cloud supersaturation from CCN measurements (CCNC method)

3.1.1 Lower bound of peak supersaturation based on CCN efficiency spectra, S_{low}(CCNC)

Figure 1 shows the size-resolved CCN efficiency spectra measured at five different supersaturation levels (S_{CCNC}) for interstitial aerosol particles in-cloud (red data points) and for total aerosol particles out-of-cloud (grey lines).

Out-of-cloud the measured CCN efficiencies (N_{CCN}/N_{CN}) exhibited the expected S-shaped increase from zero for small particles to about one for large particles. The midpoint activation diameter (D_a; at $N_{CCN}/N_{CN} = 0.5$) can be regarded as the average critical diameter of CCN activation at the given supersaturation. As expected, D_a exhibited a gradual decrease with increasing S_{CCNC}, i.e., the threshold diameter for the CCN activation of aerosol particles got lower for higher supersaturation.

In-cloud the CCN efficiency spectra observed at medium to high supersaturations were similar to those observed out-of-cloud ($S_{CCNC} \geq 0.25\,\%$, Fig. 1c–e). At low supersaturations, however, they looked very different, and the CCN efficiency of the interstitial aerosol particles remained close to zero throughout the investigated diameter range ($S_{CCNC} = 0.07\,\%$ and $0.13\,\%$, Fig. 1a and b).

From this difference we derive a lower bound for the peak supersaturation at which particles have been activated to cloud droplets (S_{low}). We take S_{low}(CCNC) to be the mean value between the highest S_{CCNC} level at which no significant activation of interstitial particles is observed ((N_{CCN}/N_{CN} – standard error) ≤ 0) and lowest S_{CCNC} level at which significant activation of interstitial particles is observed ((N_{CCN}/N_{CN} – standard error) > 0). For the investigated cloud, we thus obtained S_{low}(CCNC) = $0.19\,\% \pm 0.04\,\%$ (arithmetic mean ± standard error). Particles exhibiting critical supersaturations smaller than or equal to S_{low}(CCNC) had formed cloud droplets and

were therefore not sampled by the interstitial inlet. Hence, we did not measure activated particles in the CCNC as long as $S_{CCNC} \leq S_{low}$(CCNC). Only if S_{CCNC} exceeded S_{low}(CCNC), interstitial particles could be activated in the CCNC.

Figure 2 displays integral CCN efficiencies ($N_{CCN,int}/N_{CN,int}$; Sect. 2.5) plotted against water vapor supersaturation. It shows that S_{low}(CCNC) can be derived not only from size-resolved measurement data but also from integral measurements of CCN and CN concentrations using a combination of CCNC and CPC without DMA. In fact, even a standalone CCNC instrument and plot of $N_{CCN,int}$ vs. S_{CCNC} would suffice for the determination of S_{low}, provided that counting statistics are properly taken into account.

3.1.2 Average peak supersaturation based on CCN size distributions, S_{avg}(CCNC)

An effective average peak supersaturation (S_{avg}) at which most particles have been activated and grown into cloud droplets can be derived by comparison of CCN size distributions measured for total aerosol at different supersaturation levels with the size distribution of aerosol particles actually activated in the cloud. The number size distribution of activated particles in a cloud is given by the difference between the size distributions of total and interstitial aerosol. In principle, the particle fraction activated at a given supersaturation in the cloud should also be activated at an equivalent supersaturation level in the CCNC instrument, taking into account the influence of different ambient conditions (in particular the influence of temperature on the Kelvin effect as described in Appendix C). Consequently, the number size distribution of activated particles in a cloud should be approximately equal to the CCN size distribution measured with the CCNC for total aerosol at a supersaturation level equivalent to the effective average peak supersaturation in the cloud.

In this study we had no opportunity to measure total aerosol properties under in-cloud conditions. For the investigated cloud event, however, the in-cloud and out-of-cloud measurement periods immediately followed each other without apparent changes in the regional atmospheric conditions. Thus, we assumed the total aerosol

properties measured out-of-cloud to be approximately representative for the total aerosol properties in-cloud.

Figure 3 shows aerosol particle size distributions measured by SMPS during the investigated cloud event on 19 September 2012. For the total aerosol out-of-cloud, we observed a bimodal distribution with a minimum at ~ 65 nm. The Aitken and accumulation mode peaked at ~ 35 nm with a maximum of ~ 1700 cm^{-3} (dN/d log D) and at ~ 130 nm with a maximum of ~ 1300 cm^{-3} (dN/d log D), respectively. For the interstitial aerosol in-cloud, the Aitken mode was only slightly shifted with a maximum of ~ 1800 cm^{-3} (dN/d log D) at ~ 25 nm, whereas the accumulation mode almost disappeared because most of the larger particles had been activated into cloud droplets and could therefore not be sampled by the interstitial inlet. Figure 4 shows the size distribution of aerosol particles activated in the cloud in comparison to CCN size distributions at S_{CCNC} = 0.25 %, 0.51 % and 0.68 %. The size distribution of aerosol particles activated in the cloud was calculated by subtraction of the interstitial aerosol size distribution measured in-cloud from the total aerosol size distribution measured out-of-cloud. The number size distribution of activated particles exhibited a large peak at ~ 120 nm with a maximum of ~ 1200 cm^{-3} (dN/d log D) and a shoulder at ~ 40 nm and ~ 500 cm^{-3} (dN/d log D). The shoulder resulted from a slight shift of the CN size distribution between in-cloud and out-of-cloud conditions, which is likely due to aging processes such as condensational growth or coagulation, which are usually more pronounced for the Aitken mode than for the accumulation mode. Thus, we neglect the shoulder and exclude it from the following analysis by focusing on particles lager than 70 nm.

As shown in Fig. 4, the right-hand side of the size distribution of activated particles (D > 120 nm) is in good agreement with each of the displayed CCN size distributions. In the diameter range of 70–120 nm, however, the CCN size distribution at S_{CCNC} = 0.25 % is much lower with an average relative deviation of about −47 %. The CCN size distribution at S_{CCNC} = 0.51 % provides a fairly good match (average relative deviation +3 %) and the curve at S_{CCNC} = 0.68 % is only slightly higher (average relative deviation +11 %). Thus, we take the mean value and standard error of the three neighboring

supersaturation levels, S_{avg}(CCNC) ≈ 0.48 % ± 0.10 %, as an estimate for the effective average peak supersaturation around which most particles had been activated and most cloud droplets had been formed.

3.2 Derivation of cloud supersaturation from SMPS measurements (SMPS method)

3.2.1 Average peak supersaturation based on 50 % activation, $S_{avg}(D_{50}, \kappa)$

A common approach to derive an effective average peak supersaturation at which ambient clouds are formed is to compare the particle number or CN size distributions of total and interstitial aerosol (e.g., Anttila et al., 2009; Asmi et al., 2012; Ditas et al., 2012; Hammer et al., 2013; cf. Sect. 1). We also use this method, which will be referred to as the "SMPS method", to calculate S_{avg} from our aerosol size distribution measurement results.

In our study it was not possible to measure the particle size distribution of both interstitial and total aerosol inside the investigated cloud. As outlined above, however, we have good reasons to assume that the total aerosol size distribution measured out-of-cloud was approximately representative for the total aerosol in-cloud. A crucial point of the SMPS method is that it builds on Köhler theory calculations and requires an assumption on the hygroscopicity of the activated particles, which depends on their chemical composition. Appendix B describes how the hygroscopicity parameter κ relates the dry activation diameter of an aerosol particle to its critical supersaturation, which is the minimum supersaturation required to form a stable cloud droplet.

Figure 3 shows the CN size distribution of interstitial aerosol (red, in-cloud) and total aerosol (grey, out-of-cloud). The activated fraction (blue) was calculated by dividing the number size distribution of activated particles (out-of-cloud minus in-cloud) by the CN size distribution of the total aerosol. The diameter at which the activated fraction reached a value of 50 %, D_{50} = 58 nm, can be regarded as an effective critical dry diameter of particle activation in the cloud. By Köhler theory this diameter can be

converted into a critical supersaturation, which in turn can be regarded as an effective average peak supersaturation of the cloud (Hammer et al., 2013).

As mentioned above, the Köhler theory calculations require specific knowledge or assumptions about the hygroscopicity of the aerosol particles. Thus, we tested a range of relevant hygroscopicity parameters (κ) as specified in Appendices A and B and Table 1: (1) κ_a as determined from the measured CCN efficiency spectra during out-of-cloud conditions (κ_a = 0.17); (2) κ_{cut} as determined from the observed total CCN concentration and the CN size distribution during out-of-cloud conditions (κ_{cut} = 0.13); (3) a global average κ value for continental aerosol of κ_{mean} = 0.3 (Pringle et al., 2010); and (4) κ_{AMS} as derived from the aerosol chemical composition (κ_{AMS} = 0.45). The large difference between κ_{AMS} and κ_a or κ_{cut} can be attributed to a size-dependence of particle hygroscopicity with an enhanced organic mass fraction for sub-100 nm particles as observed in earlier studies (e.g., Gunthe et al., 2009; Gunthe et al., 2011; Rose et al., 2011). The parameter κ_{AMS} reflects the mass weighted average hygroscopicity of the total aerosol, which is dominated by large accumulation mode particles with an enhanced inorganic fraction (typically around 300 nm). Depending on the prescribed κ value, the effective average peak supersaturation derived from the SMPS-based activation curve, $S_{avg}(D_{50}, \kappa)$, was calculated to be in the range of 0.46 % to 0.84 % (arithmetic mean ± standard error: 0.65 % ± 0.08 %; Table 2). This range is consistent with the estimate derived above from the CCN measurement data without any assumption on particle hygroscopicity: S_{avg}(CCNC) ≈ 0.48 % ± 0.10 % (Sect. 3.1.2).

3.2.2 Average peak supersaturation based on the Hoppel minimum, $S_{avg}(D_H, \kappa)$

An earlier approach by Hoppel et al. (1996) derived the average cloud peak supersaturation from the shape of the aerosol size distributions typically observed in remote marine boundary layer air. The authors proposed that the double-peaked structure of the aerosol size distribution is the result of particle processing through non-precipitating cloud cycles. Thus, the diameter at which the minimum in a double-peaked particle number size distribution of total aerosol occurs ("Hoppel minimum") can be regarded

as an average critical diameter of particle activation related to the average cloud peak supersaturation.

As shown in Fig. 3, total aerosol size distribution observed out-of-cloud exhibited a very pronounced double-peak structure with a minimum at D_H = 65 nm. As described above (Sect. 3.2.1) and in Appendix B, we performed Köhler theory calculations to convert also D_H into a critical supersaturation that can be regarded as an effective average cloud peak supersaturation, assuming relevant hygroscopicity parameter values (Table 1).

Depending on the prescribed κ value, the effective average peak supersaturation derived from the Hoppel minimum diameter, $S_{avg}(D_H, \kappa)$, was calculated to be in the range of 0.38 % to 0.70 % (arithmetic mean ± standard error: 0.54 % ± 0.06 %; Table 2). This range is again consistent with the estimate derived from the CCN measurement data (S_{avg}(CCNC) ≈ 0.48 % ± 0.10 %; Sect. 3.1.2).

3.2.3 Lower bound of peak supersaturation based on full activation, $S_{low}(D_f, \kappa)$

To derive a lower bound of cloud peak supersaturation, S_{low}, from the activated particle fraction based on aerosol size distribution data, we determine an effective threshold diameter of full activation (D_f). For D_f we take the mean value between the largest diameter at which the activated fraction is significantly below unity ((activated fraction + standard error) < 1) and the smallest diameter at which practically full activation is observed ((activated fraction + standard error) ≥ 1). From Fig. 3 (blue data points) we obtained D_f = 100 nm. As described above and in Appendix B, we performed Köhler theory calculations to convert also D_f into a critical supersaturation, which can be regarded as a lower bound of cloud peak supersaturation, assuming relevant hygroscopicity parameter values (Table 1). Depending on the prescribed κ values, $S_{low}(D_f,\kappa)$ was calculated to be between 0.20 % and 0.25 % (arithmetic mean ± standard error: 0.23 % ± 0.01 %; Table 2). This range is consistent with the estimate derived from the CCN measurement data (S_{low}(CCNC) = 0.19 % ± 0.06 %).

3.2.4 Upper bound of peak supersaturation based on zero activated fraction, $S_{high}(D_0, \kappa)$

To derive an upper bound of cloud peak supersaturation, S_{high}, from the activated particle fraction based on aerosol size distribution data, we determine an effective threshold diameter of zero activation (D_0). For D_0 we take the mean value between the largest diameter at which no significant activation is observed ((activated fraction – standard error) ≤ 0) and the smallest diameter at which the activated fraction is significantly above zero ((activated fraction – standard error) > 0). From Fig. 3 (blue data points) we obtained D_0 = 37 nm. As described above and in Appendix B, we performed Köhler theory calculations to convert also D_0 into a critical supersaturation that can be regarded as an upper bound of cloud peak supersaturation, assuming relevant hygroscopicity parameter values (Table 1). Depending on the prescribed κ values, $S_{high}(D_0, \kappa)$ was calculated to be between 0.9 % and 1.64 % (arithmetic mean ± standard error: 1.27 % ± 0.15 %; Table 2).

4 Conclusions and outlook

In this study we showed how size-resolved measurements of aerosol particles and CCN in-cloud and out-of-cloud can be used to derive effective average values as well as lower and upper bounds of cloud peak supersaturation. For the investigated cloud event, the different estimates obtained from CCNC and SMPS measurement data of total and interstitial aerosol particles are largely consistent with each other (Table 2).

The uncertainties of the presented estimates of cloud peak supersaturation are mostly due to limitations in the time resolution and counting statistics of the applied measurement devices (CCNC, CPC, SMPS). Estimates derived from SMPS data only are also influenced by uncertainties in the determination or assumption of aerosol hygroscopicity parameters.

In future studies the uncertainties can and shall be reduced by optimizing the applied instrumentation and measurement procedures. Specific options for improvement are:

1. Parallel operation of total and interstitial aerosol inlets and SMPS measurements will make the determination of the fraction of aerosol particles activated in-cloud more reliable.

2. Parallel operation of multiple CCNC at different supersaturation levels and/or faster scanning of supersaturation in the CCNC by varying the flow rate rather than the temperature gradient (Moore and Nenes, 2009) will increase the number and reduce the intervals of monitored supersaturation levels and hence will increase the precision of the derived cloud peak supersaturations.

3. Increasing the aerosol-to-sheath flow ratio and/or the integration times of the CCNC and SMPS will help to improve the counting statistics.

We suggest that comprehensive measurements of the temporal and spatial variability of cloud peak supersaturation (average values as well as upper and lower bounds) may provide deeper insights into the evolution of clouds, including the interaction of aerosol and cloud particles, water vapor and dynamical features like turbulence and entrainment.

Appendix A

Calculation of κ from AMS measurements

During the ACRIDICON-Zugspitze campaign the chemical composition of submicron aerosol particles was measured with a C-ToF-AMS (Compact Time-of-Flight Aerosol Mass Spectrometer; Drewnick et al., 2005; Canagaratna et al., 2007). The C-ToF-AMS quantitatively determines the mass concentration of non-refractory species like organics, sulfate, nitrate, ammonium, and chloride. For the analysis of the cloud event

investigated in this study, the AMS mass concentrations were averaged over the time period of out-of-cloud conditions (19 September 2013 19:56–20:43 UTC). The organic (f_{org}) and inorganic mass fractions (f_{inorg}) were calculated by dividing the organic and inorganic (sum of sulfate, nitrate, ammonium, and chloride) mass concentrations by the sum of the masses of all AMS measured components, respectively.

To describe the influence of chemical composition on the CCN activity of aerosol particles Petters and Kreidenweis (2007) proposed to use a so-called hygroscopicity parameter κ. The hygroscopicity parameter (κ_{AMS}) was approximated from the AMS obtained mass fraction by a simple mixing rule as follows:

$$\kappa_{AMS} = f_{org} \cdot \kappa_{org} + f_{inorg} \cdot \kappa_{inorg} \quad \text{(A1)}$$

in which κ_{org} and κ_{inorg} are the hygroscopicity parameters for pure organic and inorganic substances (κ_{org} = 0.1 and κ_{inorg} = 0.6) (Gunthe et al., 2009; Dusek et al., 2010; Rose et al., 2011) For the average AMS derived hygroscopicity parameter we obtained κ_{AMS} = 0.45. It reflects the mass weighted average hygroscopicity of the total aerosol, which is dominated by large accumulation mode particles with an enhanced inorganic fraction (typically around 300 nm).

Appendix B

Köhler theory and calculation of κ from CCN measurements

The Köhler theory relates the dry diameter of an aerosol particle to its critical water vapor supersaturation, i.e., to the minimum supersaturation that is required to form a stable cloud droplet (Köhler, 1936). The following κ–Köhler equation (equivalent to Eq. 6 of Petters and Kreidenweis, 2007) enables to calculate the critical supersaturation (S_{crit}) for a given pair of dry particle diameter D and hygroscopicity parameter κ, or the κ parameter for a given pair of critical supersaturation and activation diameter:

$$S = \left(\frac{D_{wet}^3 - D^3}{D_{wet}^3 - D^3(1-\kappa)} \exp\left(\frac{4\sigma M_w}{RT\rho_w D_{wet}} \right) - 1 \right) \cdot 100\,\% \quad \text{(B1)}$$

where D_{wet} is the diameter of the droplet, σ is the surface tension of the droplet (approximated by that of water, $\sigma = 0.072\,J\,m^{-2}$), M_w is the molar mass of water ($M_w = 0.018015\,kg\,mol^{-1}$), R is the universal gas constant ($R = 8.315\,J\,K^{-1}\,mol^{-1}$), and ρ_w is the density of water ($\rho_w = 997.1\,kg\,m^{-3}$).

In this study, two approaches were tested to derive κ from the CCN measurement results. Firstly, the hygroscopicity parameter κ was determined from Eq. (B1) by inserting the activation diameter D_a (Sect. 3.1.1) derived from the CCN efficiency spectra measured out-of-cloud (Fig. 1) for D and varying both κ and the droplet diameter D_{wet} until S was at the same time equal to the prescribed supersaturation S_{presc} and to the maximum of Eq. B1 (cf., Rose et al., 2010). The temperature T used in Eq. (B1) was set to the value at which the particles were activated in the CCNC ($\sim 298\,K$).

A range of κ_a values between 0.17 and 0.48 was obtained for the different combinations of S_{presc} and D_a (highest values for low S_{presc}, i.e., large D_a). The parameter κ_a characterizes the average hygroscopicity of CCN-active particles in the size range around D_a. Thus, for the calculations performed in this study we assumed $\kappa_a = 0.4$ for $D \sim 100\,nm$ and $\kappa_a = 0.17$ for $D \leq 70\,nm$ (Table 1).

Alternatively, the activation diameter and corresponding hygroscopicity parameter were derived from the integral CCN concentration and the CN size distribution out-of-cloud (cf. Sect. 2.5). The apparent cut-off diameter of CCN activation (D_{cut}) is the diameter above which the integral CN number concentration equals the observed integral CCN concentration ($N_{CCN,int}$). This is equivalent to the activation diameter obtained typically from integral CCN measurements (without size-resolution), which was used also e.g. by Hammer et al. (2013).

The hygroscopicity parameter κ_{cut} was determined from Eq. (B1) by inserting the activation diameter D_{cut} for D and varying both κ and the droplet diameter D_{wet} until S was

at the same time equal to the prescribed supersaturation S_{presc} and to the maximum of Eq. (B1). The temperature T used in Eq. (B1) was set to 298 K. For the example measurement period of our study a range of κ_{cut} values between 0.13 and 0.52 was obtained for the different combinations of S_{presc} and D_{cut} (highest values for low S_{presc}, i.e., large D_{cut}). The parameter κ_{cut} characterizes the average hygroscopicity of CCN-active particles in the size range around D_{cut}. Differences between κ_a and κ_{cut} result mainly from the shape of the particle number size distribution and from the heterogeneity of the particle composition, and have been discussed in detail by Rose et al. (2010). For the calculations performed in this study we assumed $\kappa_{cut} = 0.29$ for $D \sim 100\,nm$ and $\kappa_{cut} = 0.13$ for $D \leq 70\,nm$ (Table 1).

In Sect. 3.2 of this paper, the critical supersaturation (S_{crit}) as calculated from different pairs of observed dry activation diameters and prescribed κ values was related to the cloud supersaturation. It was determined from Eq. (B1) by inserting the above-mentioned κ values (κ_a, κ_{cut}, κ_{AMS}, and $\kappa_{mean} = 0.3$) and varying both S and the droplet diameter D_{wet} until D was at the same time equal to the observed activation diameter and to the maximum of Eq. (B1). The temperature T used in Eq. (B1) had to be set to the value at which the cloud was formed in the atmospheric air. It was assumed to be $\sim 273\,K$, which was the average ambient air temperature during the cloud event.

Appendix C

Temperature scaling of supersaturation

Due to the temperature dependence of the Kelvin effect, the critical supersaturation (S_{crit}) for the CCN activation of an aerosol particle depends not only on its size and composition, but also on the temperature at which the activation occurs. Thus, the supersaturation level at which a particle is activated at ambient temperature in a cloud is not necessarily the same as the supersaturation level at which the particle is activated at instrument temperature in a CCNC.

To compensate for this effect, the supersaturation levels prescribed in the CCNC at a sample temperature of approximately 298 K (S_{presc}) were scaled to an equivalent supersaturation at an average ambient air temperature during the cloud event of ~ 273 K (S_{CCNC}).

For this purpose we performed Köhler theory calculations of S_{crit} as a function of dry particle diameter for different hygroscopicity parameter values and temperatures (Fig. C1). For a given particle diameter, the relative difference of S_{crit} at 273 K vs. 298 K was +14 % independent of the other variables (S = 0.06–0.7 %; D = 50–200 nm, κ = 0.1–0.6). Thus, we multiplied the supersaturation levels prescribed in the CCNC at ~ 298 K (S_{presc} = 0.06 %, 0.11 %, 0.22 %, 0.45 %, 0.60 %) by a factor of 1.14 to obtain the equivalent supersaturation levels for CCN activation in a cloud at ~ 273 K (S_{CCNC} = 0.07 %, 0.13 %, 0.25 %, 0.51 %, and 0.68 %), which were used for the derivation of the cloud peak supersaturation as specified in Sect. 3.1.

Acknowledgements. This work has been supported by the Max Planck Society (MPG), the Max Planck Graduate Center with the Johannes Gutenberg University Mainz (MPGC), and the German Research Foundation (DFG-SPP 1294-HALO, grant PO 1013/2). We thank D. Rosenow, M. Wendisch, and the ACRIDICON-Zugspitze team for collaboration and support. The team of the Environmental Research Station Schneefernerhaus (UFS) is acknowledged for logistical support and access to the Schneefernerhaus field site. The authors wish to thank K. Reinmuth-Selzle, C. Pöhlker, S. S. Gunthe, E. Mikhailov, L. M. Russell, M. Gysel, E. Hammer, F. Ditas, A. Wiedensohler and M. Schäfer for support and stimulating discussions.

The service charges for this open access publication
have been covered by the Max Planck Society.

References

Andreae, M. O. and Rosenfeld, D.: Aerosol-cloud-precipitation interactions. Part 1. The nature and sources of cloud-active aerosols, Earth-Sci. Rev., 89, 13–41, doi:10.1016/j.earscirev.2008.03.001, 2008.

Anttila, T., Vaattovaara, P., Komppula, M., Hyvärinen, A.-P., Lihavainen, H., Kerminen, V.-M., and Laaksonen, A.: Size-dependent activation of aerosols into cloud droplets at a subarctic background site during the second Pallas Cloud Experiment (2nd PaCE): method development and data evaluation, Atmos. Chem. Phys., 9, 4841–4854, doi:10.5194/acp-9-4841-2009, 2009.

Anttila, T., Brus, D., Jaatinen, A., Hyvärinen, A.-P., Kivekäs, N., Romakkaniemi, S., Komppula, M., and Lihavainen, H.: Relationships between particles, cloud condensation nuclei and cloud droplet activation during the third Pallas Cloud Experiment, Atmos. Chem. Phys., 12, 11435–11450, doi:10.5194/acp-12-11435-2012, 2012.

Asmi, E., Freney, E., Hervo, M., Picard, D., Rose, C., Colomb, A., and Sellegri, K.: Aerosol cloud activation in summer and winter at puy-de-Dôme high altitude site in France, Atmos. Chem. Phys., 12, 11589–11607, doi:10.5194/acp-12-11589-2012, 2012.

Canagaratna, M. R., Jayne, J. T., Jimenez, J. L., Allan, J. D., Alfarra, M. R., Zhang, Q., Onasch, T. B., Drewnick, F., Coe, H., Middlebrook, A., Delia, A., Williams, L. R., Trimborn, A. M., Northway, M. J., DeCarlo, P. F., Kolb, C. E., Davidovits, P., and Worsnop, D. R.: Chemical and microphysical characterization of ambient aerosols with the aerodyne aerosol mass spectrometer, Mass Spectrom. Rev., 26, 185–222, doi:10.1002/mas.20115, 2007.

Christensen, S. I. and Petters, M. D.: The role of temperature in cloud droplet activation, J. Phys. Chem. A, 116, 9706–9717, doi:10.1021/jp3064454, 2012.

Ditas, F., Shaw, R. A., Siebert, H., Simmel, M., Wehner, B., and Wiedensohler, A.: Aerosols-cloud microphysics-thermodynamics-turbulence: evaluating supersaturation in a marine stratocumulus cloud, Atmos. Chem. Phys., 12, 2459–2468, doi:10.5194/acp-12-2459-2012, 2012.

Drewnick, F., Hings, S. S., DeCarlo, P., Jayne, J. T., Gonin, M., Fuhrer, K., Weimer, S., Jimenez, J. L., Demerjian, K. L., Borrmann, S., and Worsnop, D. R.: A new time-of-flight aerosol mass spectrometer (TOF-AMS) – instrument description and first field deployment, Aerosol Sci. Tech., 39, 637–658, doi:10.1080/02786820500182040, 2005.

Dusek, U., Frank, G. P., Hildebrandt, L., Curtius, J., Schneider, J., Walter, S., Chand, D., Drewnick, F., Hings, S., Jung, D., Borrmann, S., and Andreae, M. O.: Size matters more than chemistry for cloud-nucleating ability of aerosol particles, Science, 312, 1375–1378, doi:10.1126/science.1125261, 2006.

Dusek, U., Frank, G. P., Curtius, J., Drewnick, F., Schneider, J., Kurten, A., Rose, D., Andreae, M. O., Borrmann, S., and Poschl, U.: Enhanced organic mass fraction and decreased hygroscopicity of cloud condensation nuclei (CCN) during new particle formation events, Geophys. Res. Lett., 37, doi:10.1029/2009gl040930, 2010.

Engelhart, G. J., Hennigan, C. J., Miracolo, M. A., Robinson, A. L., and Pandis, S. N.: Cloud condensation nuclei activity of fresh primary and aged biomass burning aerosol, Atmos. Chem. Phys., 12, 7285–7293, doi:10.5194/acp-12-7285-2012, 2012.

Frank, G. P., Dusek, U., and Andreae, M. O.: Technical note: A method for measuring size-resolved CCN in the atmosphere, Atmos. Chem. Phys. Discuss., 6, 4879–4895, doi:10.5194/acpd-6-4879-2006, 2006.

Gerber, H.: Direct measurement of suspended particulate volume concentration and far-infrared extinction coefficient with a laser-diffraction instrument, Appl. Optics, 30, 4824–4831, 1991.

Gunthe, S. S., King, S. M., Rose, D., Chen, Q., Roldin, P., Farmer, D. K., Jimenez, J. L., Artaxo, P., Andreae, M. O., Martin, S. T., and Pöschl, U.: Cloud condensation nuclei in pristine tropical rainforest air of Amazonia: size-resolved measurements and modeling of atmospheric aerosol composition and CCN activity, Atmos. Chem. Phys., 9, 7551–7575, doi:10.5194/acp-9-7551-2009, 2009.

Gunthe, S. S., Rose, D., Su, H., Garland, R. M., Achtert, P., Nowak, A., Wiedensohler, A., Kuwata, M., Takegawa, N., Kondo, Y., Hu, M., Shao, M., Zhu, T., Andreae, M. O., and Pöschl, U.: Cloud condensation nuclei (CCN) from fresh and aged air pollution in the megacity region of Beijing, Atmos. Chem. Phys., 11, 11023–11039, doi:10.5194/acp-11-11023-2011, 2011.

Hammer, E., Bukowiecki, N., Gysel, M., Jurányi, Z., Hoyle, C. R., Vogt, R., Baltensperger, U., and Weingartner, E.: Investigation of the effective peak supersaturation for liquid-phase clouds at the high-alpine site Jungfraujoch, Switzerland (3580 m a.s.l.), Atmos. Chem. Phys. Discuss., 13, 20419–20462, doi:10.5194/acpd-13-20419-2013, 2013.

Henning, S., Weingartner, E., Schmidt, S., Wendisch, M., Gaggeler, H. W., and Baltensperger, U.: Size-dependent aerosol activation at the high-alpine site Jungfraujoch (3580 m a.s.l.), Tellus B, 54, 82–95, doi:10.1034/j.1600-0889.2002.00299.x, 2002.

Hoppel, W. A., Frick, G. M., and Fitzgerald, J. W.: Deducing droplet concentration and supersaturation in marine boundary layer clouds from surface aerosol measurements, J. Geophys. Res.-Atmos., 101, 26553–26565, doi:10.1029/96jd02243, 1996.

Jurányi, Z., Gysel, M., Weingartner, E., DeCarlo, P. F., Kammermann, L., and Baltensperger, U.: Measured and modelled cloud condensation nuclei number concentration at the high alpine site Jungfraujoch, Atmos. Chem. Phys., 10, 7891–7906, doi:10.5194/acp-10-7891-2010, 2010.

Jurányi, Z., Tritscher, T., Gysel, M., Laborde, M., Gomes, L., Roberts, G., Baltensperger, U., and Weingartner, E.: Hygroscopic mixing state of urban aerosol derived from size-resolved cloud condensation nuclei measurements during the MEGAPOLI campaign in Paris, Atmos. Chem. Phys., 13, 6431–6446, doi:10.5194/acp-13-6431-2013, 2013.

Kim, J. H., Yum, S. S., Shim, S., Yoon, S.-C., Hudson, J. G., Park, J., and Lee, S.-J.: On aerosol hygroscopicity, cloud condensation nuclei (CCN) spectra and critical supersaturation measured at two remote islands of Korea between 2006 and 2009, Atmos. Chem. Phys., 11, 12627–12645, doi:10.5194/acp-11-12627-2011, 2011.

Kinne, S.: Climatologies of cloud-related aerosol, Part 1: particle number and size, in: Clouds in the Perturbed Climate System: their Relationship to Energy Balance, Atmospheric Dynamics, and Precipitation, edited by: Heintzenberg, J. and Charlson, R. J., MIT Press, Cambridge, MA, USA, 37–57, 2009.

Köhler, H.: The nucleus in and the growth of hygroscopic droplets, T. Faraday Soc., 32, 1152–1161, doi:10.1039/tf9363201152, 1936.

Kulmala, M., Asmi, A., Lappalainen, H. K., Baltensperger, U., Brenguier, J.-L., Facchini, M. C., Hansson, H.-C., Hov, Ø., O'Dowd, C. D., Pöschl, U., Wiedensohler, A., Boers, R., Boucher, O., de Leeuw, G., Denier van der Gon, H. A. C., Feichter, J., Krejci, R., Laj, P., Lihavainen, H., Lohmann, U., McFiggans, G., Mentel, T., Pilinis, C., Riipinen, I., Schulz, M., Stohl, A., Swietlicki, E., Vignati, E., Alves, C., Amann, M., Ammann, M., Arabas, S., Artaxo, P., Baars, H., Beddows, D. C. S., Bergström, R., Beukes, J. P., Bilde, M., Burkhart, J. F., Canonaco, F., Clegg, S. L., Coe, H., Crumeyrolle, S., D'Anna, B., Decesari, S., Gilardoni, S., Fischer, M., Fjaeraa, A. M., Fountoukis, C., George, C., Gomes, L., Halloran, P., Hamburger, T., Harrison, R. M., Herrmann, H., Hoffmann, T., Hoose, C., Hu, M., Hyvärinen, A., Hõrrak, U., Iinuma, Y., Iversen, T., Josipovic, M., Kanakidou, M., Kiendler-Scharr, A., Kirkevåg, A., Kiss, G., Klimont, Z., Kolmonen, P., Komppula, M., Kristjánsson, J.-E., Laakso, L., Laaksonen, A., Labonnote, L., Lanz, V. A., Lehtinen, K. E. J., Rizzo, L. V.,

Makkonen, R., Manninen, H. E., McMeeking, G., Merikanto, J., Minikin, A., Mirme, S., Morgan, W. T., Nemitz, E., O'Donnell, D., Panwar, T. S., Pawlowska, H., Petzold, A., Pienaar, J. J., Pio, C., Plass-Duelmer, C., Prévôt, A. S. H., Pryor, S., Reddington, C. L., Roberts, G., Rosenfeld, D., Schwarz, J., Seland, Ø., Sellegri, K., Shen, X. J., Shiraiwa, M., Siebert, H., Sierau, B., Simpson, D., Sun, J. Y., Topping, D., Tunved, P., Vaattovaara, P., Vakkari, V., Veefkind, J. P., Visschedijk, A., Vuollekoski, H., Vuolo, R., Wehner, B., Wildt, J., Woodward, S., Worsnop, D. R., van Zadelhoff, G.-J., Zardini, A. A., Zhang, K., van Zyl, P. G., Kerminen, V.-M., S Carslaw, K., and Pandis, S. N.: General overview: European Integrated project on Aerosol Cloud Climate and Air Quality interactions (EUCAARI) – integrating aerosol research from nano to global scales, Atmos. Chem. Phys., 11, 13061–13143, doi:10.5194/acp-11-13061-2011, 2011.

Lance, S., Raatikainen, T., Onasch, T. B., Worsnop, D. R., Yu, X.-Y., Alexander, M. L., Stolzenburg, M. R., McMurry, P. H., Smith, J. N., and Nenes, A.: Aerosol mixing state, hygroscopic growth and cloud activation efficiency during MIRAGE 2006, Atmos. Chem. Phys., 13, 5049–5062, doi:10.5194/acp-13-5049-2013, 2013.

Lohmann, U. and Feichter, J.: Global indirect aerosol effects: a review, Atmos. Chem. Phys., 5, 715–737, doi:10.5194/acp-5-715-2005, 2005.

McFiggans, G., Artaxo, P., Baltensperger, U., Coe, H., Facchini, M. C., Feingold, G., Fuzzi, S., Gysel, M., Laaksonen, A., Lohmann, U., Mentel, T. F., Murphy, D. M., O'Dowd, C. D., Snider, J. R., and Weingartner, E.: The effect of physical and chemical aerosol properties on warm cloud droplet activation, Atmos. Chem. Phys., 6, 2593–2649, doi:10.5194/acp-6-2593-2006, 2006.

Mertes, S., Lehmann, K., Nowak, A., Massling, A., and Wiedensohler, A.: Link between aerosol hygroscopic growth and droplet activation observed for hill-capped clouds at connected flow conditions during FEBUKO, Atmos. Environ., 39, 4247–4256, doi:10.1016/j.atmosenv.2005.02.010, 2005.

Mikhailov, E., Vlasenko, S., Rose, D., and Pöschl, U.: Mass-based hygroscopicity parameter interaction model and measurement of atmospheric aerosol water uptake, Atmos. Chem. Phys., 13, 717–740, doi:10.5194/acp-13-717-2013, 2013.

Moore, R. H. and Nenes, A.: Scanning flow CCN analysis – a method for fast measurements of CCN spectra, Aerosol Sci. Tech., 43, 1192–1207, doi:10.1080/02786820903289780, 2009.

Padró, L. T., Moore, R. H., Zhang, X., Rastogi, N., Weber, R. J., and Nenes, A.: Mixing state and compositional effects on CCN activity and droplet growth kinetics of size-resolved CCN in

an urban environment, Atmos. Chem. Phys., 12, 10239–10255, doi:10.5194/acp-12-10239-2012, 2012.

Petters, M. D. and Kreidenweis, S. M.: A single parameter representation of hygroscopic growth and cloud condensation nucleus activity, Atmos. Chem. Phys., 7, 1961–1971, 2007, http://www.atmos-chem-phys.net/7/1961/2007/.

Petters, M. D. and Kreidenweis, S. M.: A single parameter representation of hygroscopic growth and cloud condensation nucleus activity – Part 2: Including solubility, Atmos. Chem. Phys., 8, 6273–6279, doi:10.5194/acp-8-6273-2008, 2008.

Petters, M. D. and Kreidenweis, S. M.: A single parameter representation of hygroscopic growth and cloud condensation nucleus activity – Part 3: Including surfactant partitioning, Atmos. Chem. Phys., 13, 1081–1091, doi:10.5194/acp-13-1081-2013, 2013.

Pöschl, U.: Atmospheric aerosols: composition, transformation, climate and health effects, Angew. Chem. Int. Edit., 44, 7520–7540, doi:10.1002/anie.200501122, 2005.

Pöschl, U., Rose, D., and Andreae, M. O.: Climatologies of cloud-related aerosols, Part 2: particle hygroscopicity and cloud condensation nucleus activity, in: Clouds in the Perturbed Climate System: their Relationship to Energy Balance, Atmospheric Dynamics, and Precipitation, edited by: Heintzenberg, J. and Charlson, R. J., MIT Press, Cambridge, MA, USA, 57–72, 2009.

Pringle, K. J., Tost, H., Pozzer, A., Pöschl, U., and Lelieveld, J.: Global distribution of the effective aerosol hygroscopicity parameter for CCN activation, Atmos. Chem. Phys., 10, 5241–5255, doi:10.5194/acp-10-5241-2010, 2010.

Pruppacher, H. R. and Klett, J. D.: Microphysics of Clouds and Precipitation, Atmospheric and Oceanographic Sciences Library, 18, Springer, Netherlands, 954 pp., 2010.

Renno, N. O., Williams, E., Rosenfeld, D., Fischer, D. G., Fischer, J., Kremic, T., Agrawal, A., Andreae, M. O., Bierbaum, R., Blakeslee, R., Boerner, A., Bowles, N., Christian, H., Cox, A., Dunion, J., Horvath, A., Huang, X. L., Khain, A., Kinne, S., Lemos, M. C., Penner, J. E., Poschl, U., Quaas, J., Seran, E., Stevens, B., Walati, T., and Wagner, T.: CHASER – an innovative satellite mission concept to measure the effects of aerosols on clouds and climate, B. Am. Meteorol. Soc., 94, 685–694, doi:10.1175/bams-d-11-00239.1, 2013.

Reutter, P., Su, H., Trentmann, J., Simmel, M., Rose, D., Gunthe, S. S., Wernli, H., Andreae, M. O., and Pöschl, U.: Aerosol- and updraft-limited regimes of cloud droplet formation: influence of particle number, size and hygroscopicity on the activation of cloud condensation nuclei (CCN), Atmos. Chem. Phys., 9, 7067–7080, doi:10.5194/acp-9-7067-2009, 2009.

Roberts, G. C. and Nenes, A.: A continuous-flow streamwise thermal-gradient CCN chamber for atmospheric measurements, Aerosol Sci. Tech., 39, 206–221, doi:10.1080/027868290913988, 2005.

Rose, D., Gunthe, S. S., Mikhailov, E., Frank, G. P., Dusek, U., Andreae, M. O., and Pöschl, U.: Calibration and measurement uncertainties of a continuous-flow cloud condensation nuclei counter (DMT-CCNC): CCN activation of ammonium sulfate and sodium chloride aerosol particles in theory and experiment, Atmos. Chem. Phys., 8, 1153–1179, doi:10.5194/acp-8-1153-2008, 2008.

Rose, D., Nowak, A., Achtert, P., Wiedensohler, A., Hu, M., Shao, M., Zhang, Y., Andreae, M. O., and Pöschl, U.: Cloud condensation nuclei in polluted air and biomass burning smoke near the mega-city Guangzhou, China – Part 1: Size-resolved measurements and implications for the modeling of aerosol particle hygroscopicity and CCN activity, Atmos. Chem. Phys., 10, 3365–3383, doi:10.5194/acp-10-3365-2010, 2010.

Rose, D., Gunthe, S. S., Su, H., Garland, R. M., Yang, H., Berghof, M., Cheng, Y. F., Wehner, B., Achtert, P., Nowak, A., Wiedensohler, A., Takegawa, N., Kondo, Y., Hu, M., Zhang, Y., Andreae, M. O., and Pöschl, U.: Cloud condensation nuclei in polluted air and biomass burning smoke near the mega-city Guangzhou, China – Part 2: Size-resolved aerosol chemical composition, diurnal cycles, and externally mixed weakly CCN-active soot particles, Atmos. Chem. Phys., 11, 2817–2836, doi:10.5194/acp-11-2817-2011, 2011.

Rosenfeld, D., Lohmann, U., Raga, G. B., O'Dowd, C. D., Kulmala, M., Fuzzi, S., Reissell, A., and Andreae, M. O.: Flood or drought: how do aerosols affect precipitation?, Science, 321, 1309–1313, doi:10.1126/science.1160606, 2008.

Rosenfeld, D., Williams, E., Andreae, M. O., Freud, E., Pöschl, U., and Rennó, N. O.: The scientific basis for a satellite mission to retrieve CCN concentrations and their impacts on convective clouds, Atmos. Meas. Tech., 5, 2039–2055, doi:10.5194/amt-5-2039-2012, 2012.

Russell, L. M., Sorooshian, A., Seinfeld, J. H., Albrecht, B. A., Nenes, A., Ahlm, L., Chen, Y.-C., Coggon, M., Craven, J. S., Flagan, R. C., Frossard, A. A., Jonsson, H., Jung, E., Lin, J. J., Metcalf, A. R., Modini, R., Mülmenstädt, J., Roberts, G., Shingler, T., Song, S., Wang, Z., and Wonaschütz, A.: Eastern Pacific Emitted Aerosol Cloud Experiment, B. Am. Meteorol. Soc., 94, 709–729, doi:10.1175/BAMS-D-12-00015.1, 2013.

Solomon, S., Qin, D., Manning, Z., Chen, Z., Marquis, M., Avery, K. B., Tignor, M., and Miller, H. L. E.: IPCC 4th Assessment Report, Cambridge Univ. Press, Cambridge, 2007.

Spracklen, D. V., Carslaw, K. S., Pöschl, U., Rap, A., and Forster, P. M.: Global cloud condensation nuclei influenced by carbonaceous combustion aerosol, Atmos. Chem. Phys., 11, 9067–9087, doi:10.5194/acp-11-9067-2011, 2011.

Su, H., Rose, D., Cheng, Y. F., Gunthe, S. S., Massling, A., Stock, M., Wiedensohler, A., Andreae, M. O., and Pöschl, U.: Hygroscopicity distribution concept for measurement data analysis and modeling of aerosol particle mixing state with regard to hygroscopic growth and CCN activation, Atmos. Chem. Phys., 10, 7489–7503, doi:10.5194/acp-10-7489-2010, 2010.

Wex, H., McFiggans, G., Henning, S., and Stratmann, F.: Influence of the external mixing state of atmospheric aerosol on derived CCN number concentrations, Geophys. Res. Lett., 37, L10805, doi:10.1029/2010gl043337, 2010.

Table 1. Different combinations of hygroscopicity parameters (κ_a, κ_{cut}, κ_{mean}, κ_{AMS}) and activation threshold diameters (D_f, D_{50}, D_H, D_0) used to determine the cloud peak supersaturations reported in Table 2 by Köhler theory calculations as detailed in Appendices A and B.

	D_f = 100.3 nm	D_{50} = 57.6 nm	D_H = 65.1 nm	D_0 = 36.6 nm
κ_a	0.4	0.17	0.17	0.17
κ_{cut}	0.29	0.13	0.13	0.13
κ_{mean}	0.3	0.3	0.3	0.3
κ_{AMS}	0.45	0.45	0.45	0.45

Table 2. Lower bounds, average values and upper bounds of cloud peak supersaturation (S_{low}, S_{avg}, S_{high}) obtained by Köhler theory calculations assuming different types of hygroscopicity parameter (κ_a, κ_{cut}, κ_{mean}, κ_{AMS}) as reported in Table 1 (SMPS method; Sect. 3.2). The values displayed in the second-last line represent the arithmetic mean ± standard error of the preceding four lines (SMPS method average). The supersaturation values displayed in the last line were obtained without assumptions about particle hygroscopicity (arithmetic mean ± standard error; CCNC method; Sect. 3.1).

	$S_{low}(D = D_f, \kappa)$ [%]	$S_{avg}(D = D_{50}, \kappa)$ [%]	$S_{avg}(D = D_H, \kappa)$ [%]	$S_{high}(D = D_0, \kappa)$ [%]
$S(D, \kappa = \kappa_a)$	0.21	0.74	0.61	1.45
$S(D, \kappa = \kappa_{cut})$	0.25	0.84	0.70	1.64
$S(D, \kappa = \kappa_{mean})$	0.24	0.56	0.46	1.10
$S(D, \kappa = \kappa_{AMS})$	0.20	0.46	0.38	0.90
S(SMPS)	0.23 ± 0.01	0.65 ± 0.08	0.54 ± 0.06	1.27 ± 0.15
S(CCNC)	0.19 ± 0.04	0.48 ± 0.10	0.48 ± 0.10	–

Table A1. Notation (frequently used symbols).

Symbol	Quantity, Unit
N_{CCN}	monodisperse number concentration of CCN at certain S, cm^{-3}
N_{CN}	monodisperse number concentration of CN, cm^{-3}
N_{CCN}/N_{CN}	CCN efficiency (size-resolved) at certain S
$N_{CCN,int}$	integral CCN concentration at certain S, cm^{-3}
$N_{CN,int}$	integral CN concentration, cm^{-3}
$N_{CCN,int}/N_{CCN,int}$	integral CCN efficiency at certain S
S	water vapor supersaturation, %
S_{presc}	supersaturation prescribed in the CCNC operated at room temperature (~ 298 K), %
S_{CCNC}	supersaturation in the CCNC scaled to cloud temperature (~ 273 K), %
S_{low}	lower bound of cloud peak supersaturation, %
S_{avg}	average value of cloud peak supersaturation, %
S_{high}	upper bound of cloud peak supersaturation, %
D	dry particle diameter, nm
D_0	diameter of zero activation observed in the cloud, nm
D_{50}	diameter of 50 % activation observed in the cloud, nm
D_H	diameter of the Hoppel minimum, nm
D_f	diameter of full activation observed in the cloud, nm
D_a	midpoint activation diameter of CCN efficiency spectrum (at N_{CCN}/N_{CN} = 0.5), nm
D_{cut}	cut-off diameter of CCN activation, nm
κ	effective hygroscopicity parameter
κ_a	hygroscopicity parameter derived from D_a via Köhler theory
κ_{cut}	hygroscopicity parameter derived from D_{cut} via Köhler theory
κ_{mean}	mean hygroscopicity parameter for continental aerosol (κ_{mean} = 0.3)
κ_{AMS}	hygroscopicity parameter derived from AMS data (κ_{AMS} = 0.45)

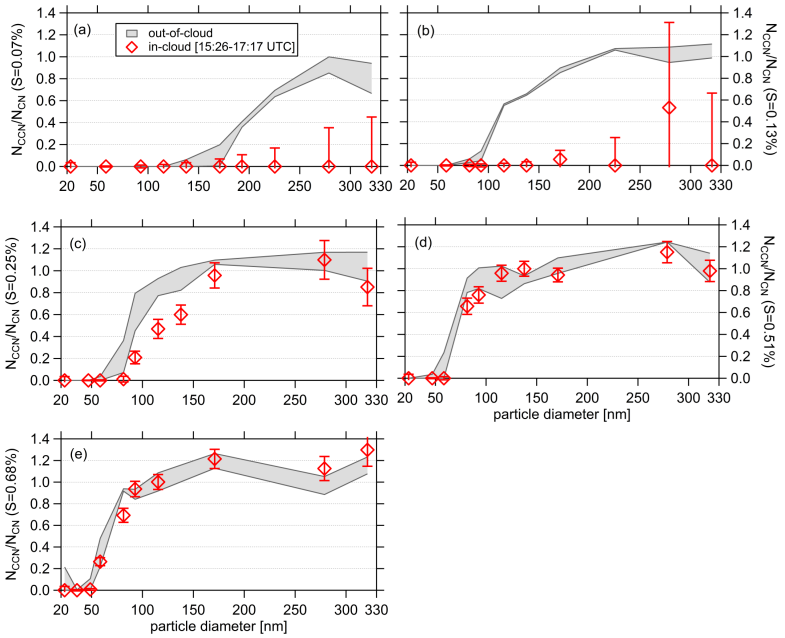

Fig. 1. Size-resolved CCN efficiency spectra measured for different S_{CCNC}. The red squares represent one example measurement during the cloud event (19 September 2012 15:26–17:17 UTC) and the error bars correspond to the individual standard errors calculated as described in Sect. 2.4. The grey shaded area represents the arithmetic mean ± standard deviation of CCN measurements performed during out-of-cloud conditions directly after the cloud event (19 September 2012 17:26–19:17 UTC and 19 September 23:26 UTC–20 September 01:17 UTC).

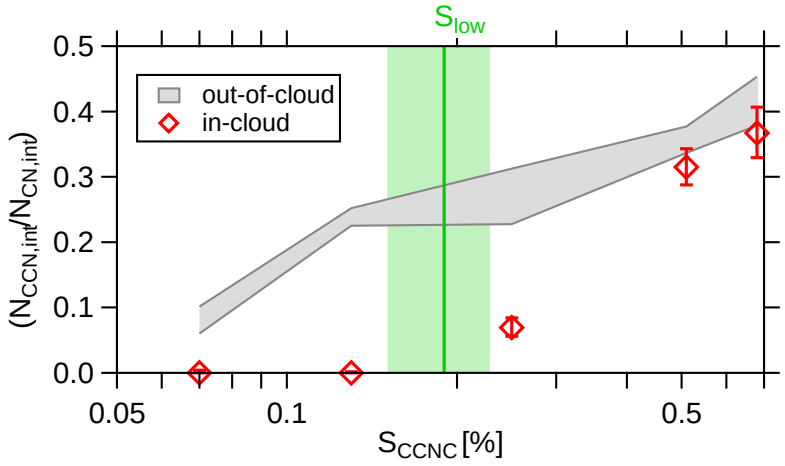

Fig. 2. Integral CCN efficiency measured for total aerosol during out-of-cloud conditions (grey shaded area; arithmetic mean ± standard deviation) and for interstitial aerosol in one example measurement during in-cloud conditions (red data points, error bars correspond to the individual standard errors) plotted as a function of S_{CCNC}. The measurement times are the same as in Fig. 1. The vertical green line and shaded area represent the arithmetic mean and standard error range of S_{low}(CCNC).

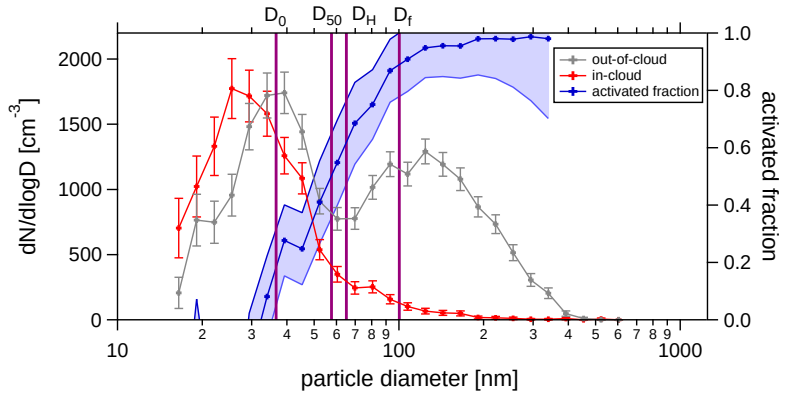

Fig. 3. Average number size distribution of total aerosol particles (grey crosses; out-of-cloud) and of interstitial aerosol particles (red crosses; in-cloud). The error bars correspond to the individual standard errors calculated as described in Sect. 2.4. The activated fraction (blue line; grey minus red, divided by grey; shaded area is the range of the statistical error of the data points) is plotted on the right axis. To assure comparability of the size distributions their averaging times were chosen to be unambiguous with respect to LWC for in-cloud (mean LWC = 0.131 g m^{-3}) and out-of-cloud conditions (mean LWC = 0.016 g m^{-3}) within a short time interval (in-cloud: 19 September 2012 15:00–16:00 UTC; out-of-cloud: 19 September 2012 17:30–18:00 UTC). The vertical lines indicate the diameters of zero activation (D_0), 50 % activation (D_{50}), Hoppel minimum (D_H), and full activation (D_f).

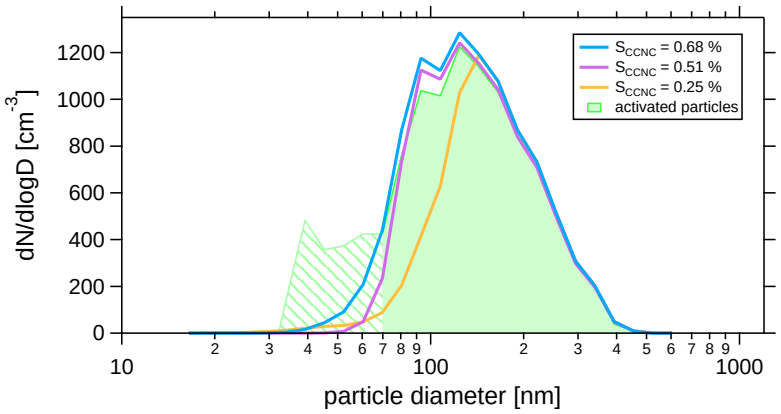

Fig. 4. Average number size distribution of activated particles in the cloud (green shaded area; hatched shoulder excluded from analysis) and CCN size distributions at S_{CCNC} = 0.25 %, 0.51 %, and 0.68 % (colored lines).

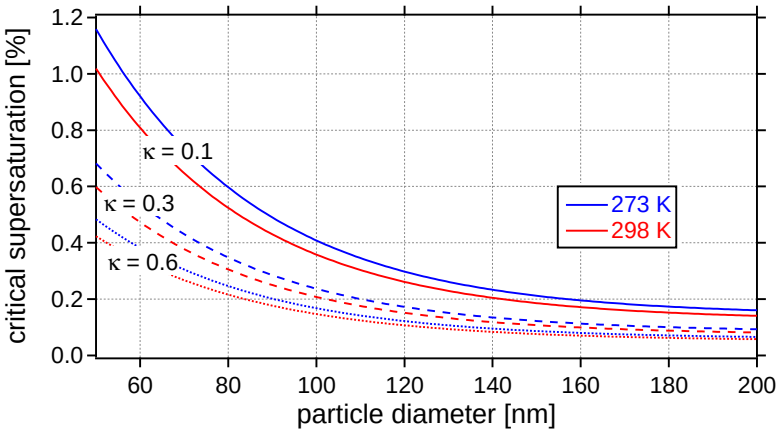

Fig. C1. Critical supersaturation as a function of dry particle diameter calculated from Köhler theory (Appendix B) using different hygroscopicity parameters and temperatures as input parameters.